International Journal of Minerals, Metallurgy and Materials
Volume 24, Number 11, November 2017, Page 1321
DOI: 10.1007/s12613-017-1524-0

CuCrW(Al_2O_3) nanocomposite: mechanical alloying, microstructure, and tribological properties

Mohammad Baghani and Mahmood Aliofkhazraei

Department of Materials Science, Faculty of Engineering, Tarbiat Modares University, Tehran, Iran, P.O. Box: 14115-143
(Received: 18 January 2017; revised: 18 May 2017; accepted: 20 May 2017)

Abstract: The effect of alumina nanoparticle addition on the microstructure and tribological properties of a CuCrW alloy was investigated in this work. Mechanical alloying was carried out in a satellite ball mill. The tribological properties of the samples were evaluated using pin-on-disk wear tests with different pins (alumina, tungsten carbide, and steel pins). The results indicated that the tungsten carbide pin had a lower coefficient of friction than the alumina and steel pins because of its high hardness and low surface roughness. In addition, when the sliding rate was decreased, the weight-loss rate increased. The existence of alumina nanoparticles in the nanocomposite led to a lower weight-loss rate and to a change in the wear mechanism from adhesive to abrasive.

Keywords: wear; mechanical alloying; nanocomposite; tribological properties; metal matrix

1. Introduction

Copper improves the mechanical properties of Cu-based alloys. Because of its excellent mechanical and electrical properties, CuCr alloy has found numerous engineering applications in cable connections, welding wire, high-voltage switches, and wear connectors [1]. The equilibrium solubility of Cr in Cu is very low even at a eutectic temperature; for example, at a temperature of 1070°C, the solid solubility capacity of Cr in Cu is only 0.8wt% [2].

Numerous studies have been conducted on procedures for preparing CuCr supersaturated solid solutions (SSs) [3–5]. Because of the difficulty involved in the preparation of CuCr supersaturated SSs using conventional metallurgical methods, researchers have developed a method of producing CuCr alloy through the non-equilibrium mechanical alloying process. This technique offers the additional benefit of increasing the solubility limit of Cr in Cu [6–8]. Sheibani *et al.* [9] examined the effect of alumina (Al_2O_3) nanoparticle addition on the development of the Cr solution in Cu through mechanical alloying. After mixing Cr and Cu powders and pure Al_2O_3 nanopowder in a ball-mill satellite, they obtained a final product of a CuCr supersaturated SS with a crystalline size range from 8 to 19 nm. They also measured the Gibbs free energy variations during the mechanical alloying process. The presence of Al_2O_3 nanoparticles affected the changes in the Gibbs free energy and triggered the increase in Cr solubility in Cu.

Adding W to Cu-based alloys also leads to improved characteristics such as increases in the alloys' density, melting point, and high-temperature strength. CuW alloys are widely applied as materials for high-voltage electrical connections, electrical discharge machining electrodes, and high-temperature molds [10]. These materials are not soluble even in the molten state because of the differences in the crystal structures, melting points, moduli of elasticity, and wettabilities of Cu and W. Cu has a high thermal expansion coefficient, which can be manipulated by adding W to Cu. As with CuCr alloys, the preparation of CuW alloys is difficult using conventional methods [11]. Bacal *et al.* have reported the electrodeposition of CuW alloy in a bath containing citrate solution [12]. They carried out the electrodeposition over a silver substrate and under constant-current conditions. The maximum W content achieved in electrop-

Corresponding author: Mahmood Aliofkhazraei E-mail: maliofkh@gmail.com, khazraei@modares.ac.ir

lated CuW alloy is 30wt% W, and the obtained alloy exhibits a microhardness of HV 400. Raghu *et al.* [13] reported the synthesis of CuW nanocrystalline alloys through mechanical alloying. They mixed Cu and W powders in a satellite ball mill under an oxygenated atmosphere. The changes in the lattice parameter indicated Cu–Zn SS formation. The resultant energy of milling resulted in a nanocrystalline and quasistable SS. Xu *et al.* [14] reported the fabrication of CuW alloy through microwave infiltration sintering under vacuum conditions. Their fabricated alloy consisted of a $Cu_{0.4}W_{0.6}$ phase, and their results showed that an increase in Cu content resulted in a lower porosity. In addition, the addition of reinforcing oxide nanoparticles to Cu-based alloys results in an improvement in either strength or wear resistance through a combination of modified grain-boundary pinning behavior and the prevention of dislocation movement [15].

Mechanical milling has been speculated to be an appropriate technique for alloying because it facilitates surface diffusion and the uniform distribution of nanoparticles in the metallic matrix and enables the synthesis of metallic matrix nanocomposites. Raju *et al.* [16] studied the effect of adding Al_2O_3 nanoparticles on the mechanical properties of $Cu–Al_2O_3$ nanocomposites. The nanocomposites were prepared via a friction stir process, which uniformly distributed the Al_2O_3 nanoparticles. Moreover, the microhardness and tensile properties of the nanocomposites increased with increasing percentage of Al_2O_3 hard particles. Accordingly, in the present study, we investigate the effect of adding α-Al_2O_3 hard nanoparticles on the microstructure and tribological properties of CuCrW alloy. Cu, W, and Cr powders with 0vol% and 5vol% of Al_2O_3 nanopowders were mixed in a satellite ball mill. The alloyed powders were pressed and sintered in a conventional furnace. The tribological features of the obtained CuCrW(Al_2O_3) nanocomposites were studied through pin-on-disk wear tests conducted under different test conditions.

2. Research methodology

The powders of pure Cu (99%, <20 μm, analytical grade), W (99%, <45 μm, analytical grade), and Cr (99%, <20 μm, analytical grade) together with Al_2O_3 nanopowders (99%, <20 nm, analytical grade) were chosen as the raw materials for alloying to prepare the nanocomposites. The particle morphology was characterized by scanning electron microscopy (SEM, Philips XL30) and transmission electron microscopy (TEM, Zeiss EMIOC). As shown in Fig. 1, the W, Cr, and Cu powder particles are irregular, spherical, and agglomerated, respectively.

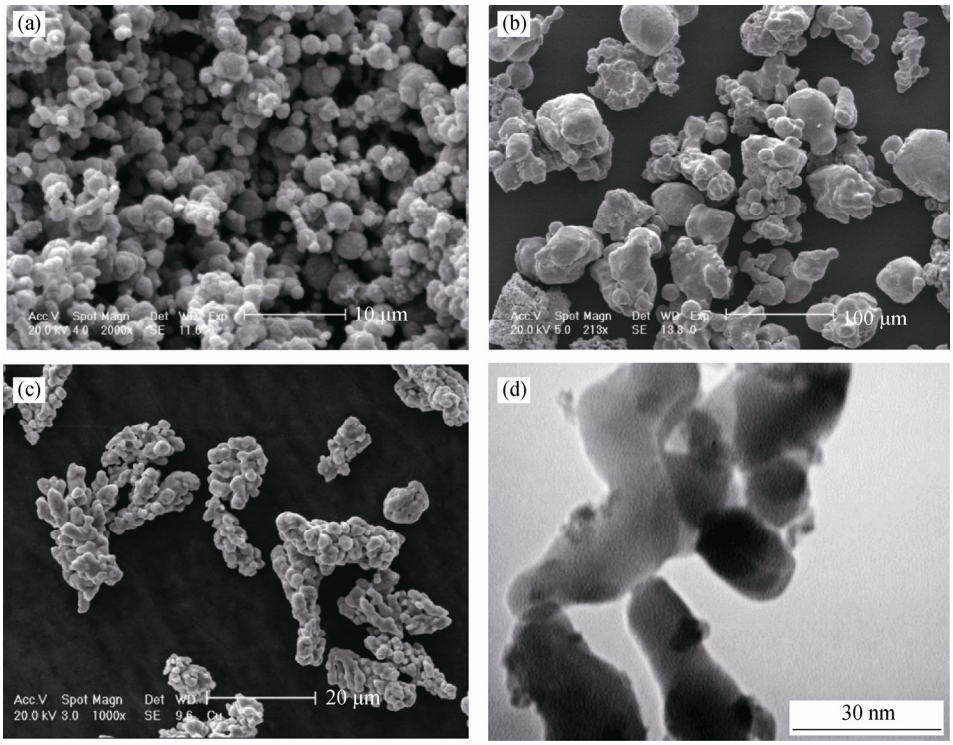

Fig. 1. SEM images of different powder particles: (a) W; (b) Cr; (c) Cu; (d) Al_2O_3 nanoparticles prior to mechanical milling.

To determine the effect of adding Al_2O_3 nanoparticles, a mixture of Cu–10wt%Cr–10wt%W powder with 0vol% and 5vol% of Al_2O_3 was subjected to mechanical alloying conditions. The milling medium for this procedure was tungsten carbide (WC). Powder mixed with 1 mL of ethanol as a process control agent was mechanically milled for 50 h with a ball-to-powder weight ratio of 10:1 and at a rotation speed of 300 r/min in a planetary ball mill under a controlled argon atmosphere.

The mechanically alloyed powders were characterized using a Philips X'Pert MPD X-ray diffractometer equipped with a Co K_α radiation source (λ = 0.1789 nm). The milled powder was pressed under a cold pressure of 350 MPa, and green compacts with a diameter and thickness of 25 and 3 mm, respectively, were prepared. The green compacts were sintered in a tube furnace at 850°C for 30 min under an argon atmosphere. The microstructures and chemical compositions of the sintered specimens' cross sections were also studied by field-emission scanning electron microscopy (FESEM) on a Zeiss AMA electron microscope. The density of the samples was determined according to the Archimedes' law (ASTM B962) at 25°C, and their hardness was measured using Vickers microhardness measurements conducted with a load of 9.8 N and a dwell time of 10 s. The tribological tests were carried out using wear tests (pin-on-disk) according to the test conditions specified in standard ASTM G99. A normal load of 10 N was applied with a radius of 10 mm. Before the wear tests, all of the samples were polished and then cleaned in an ultrasonic bath. Three types of pins were used in the wear tests: Al_2O_3, WC, and steel 52100. In the present study, Al_2O_3, WC, and steel pins were mounted on a pin holder. The surface hardness of the applied pins is presented in Table 1. Each test comprised three steps: the sliding distance was 50 m in the first step, 150 m in the second, and 300 m in the third. A Taylor–Hobson roughness tester (Surtronic 25, with 0.01-μm resolution) was used to obtain the profiles on the micrometer scale. To investigate the wear mechanism, the wear surface developed on the disk was imaged after the wear test by SEM. Test material composition and speed are presented in Table 2. Each test was performed twice to ensure repeatability.

Table 1. Mechanical parameters of the three pins used in the wear tests

Pin	Surface hardness, HV	RMS of surface roughness / μm
Alumina	1800	0.096
WC	1250	0.090
Steel	750	0.089

Note: RMS — root mean square.

Table 2. Wear test procedure

Test No.	Test conditions		
	Pin material	Disc material	Sliding speed / ($m \cdot s^{-1}$)
1	Al_2O_3	CuCrW	1
2	Al_2O_3	CuCrW	5
3	WC	CuCrW	1
4	WC	CuCrW	5
5	Steel	CuCrW	1
6	Steel	CuCrW	5
7	Al_2O_3	CuCrW(Al_2O_3)	1
8	Al_2O_3	CuCrW(Al_2O_3)	5
9	WC	CuCrW(Al_2O_3)	1
10	WC	CuCrW(Al_2O_3)	5
11	Steel	CuCrW(Al_2O_3)	1
12	Steel	CuCrW(Al_2O_3)	5

3. Results and discussion

3.1. XRD and SEM analysis

Fig. 2 shows the X-ray diffraction (XRD) patterns of the $Cu_{80}Cr_{10}W_{10}$ powder mixture at different times of mechanical alloying. During the mechanical alloying process, Cr and W atoms were gradually introduced into the Cu structure and a CuCrW SS was formed. The atomic radii of Cr, W, and Cu are 0.166, 0.193, and 0.145 nm, respectively [17]. The diffusion of Cr and W atoms into the Cu lattice increases the Cu lattice parameter and shifts the Cu peaks to lower angles in the XRD patterns. In Fig. 2, the Cu peaks indexed with planes (111) and (200) shift toward lower angles because of the diffusion of Cr and W atoms into the Cu structure and the formation of a CuCrW SS. With increasing milling time, the peak width of all elements increased, whereas the peak intensity decreased. Peak broadening results from a decrease in grain size and an increase in lattice strain [18]. Because larger strains are developed in the lattice during mechanical alloying, the Williamson–Hall method is more accurate than other methods for calculating strain [19]:

$$\beta = (0.9\lambda/d\cos\theta) + 4\varepsilon\tan\theta \quad (1)$$

where d is the crystalline grain size, β is the full-width at half-maximum of the selected peak, λ is the wavelength of the X-rays, θ is the Bragg angle, and ε is the lattice strain. By substituting the appropriate value for β into the Williamson–Hall relationship, a plot of $\beta\cos\theta$ vs. $\sin\theta$ can be constructed. We obtain the strain component from the slope and the size component from the intercept. The changes in crystalline size and lattice strain of the Cu matrix versus time of the mechanical alloying are plotted in Fig. 3. Fig. 3(a) shows the crystalline size graph versus time of me-

chanical alloying. The crystalline size decreases with increasing milling time during the mechanical alloying. As expected, the calculated size of the Cu-matrix crystals demonstrates that the severe plastic deformation of the powders during the mechanical alloying process leads to a decrease in the size of the Cu-matrix crystals to approximately 29 nm.

The final crystalline grain size derived from milling is the result of interactions between the mechanical deformation of particles and the recovery rate during the milling process. The plastic deformation and the recovery behavior of milled materials depend on their physical properties [20]. Fig. 3(b) presents the lattice strain graph relative to the mechanical alloying time. With increasing mechanical alloying time, the strain of the crystalline lattice increased, reaching 58% after 50 h. Fracture and grain rotation are expected to be the sole dominant mechanism for developing tension during the mechanical milling process [21]. The increase in lattice strain and dislocation density not only reduces the activation energy of diffusion but also leads to the creation of high-diffusivity paths [21].

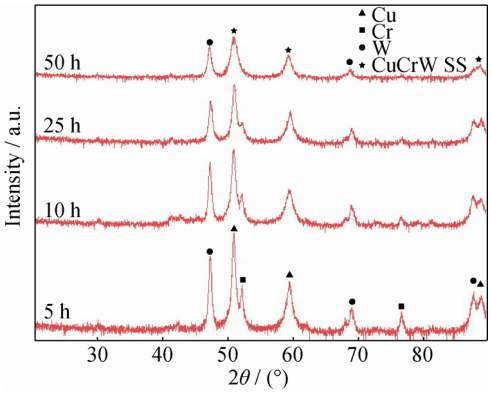

Fig. 2. XRD patterns of $Cu_{80}Cr_{10}W_{10}$ after different durations of mechanical alloying.

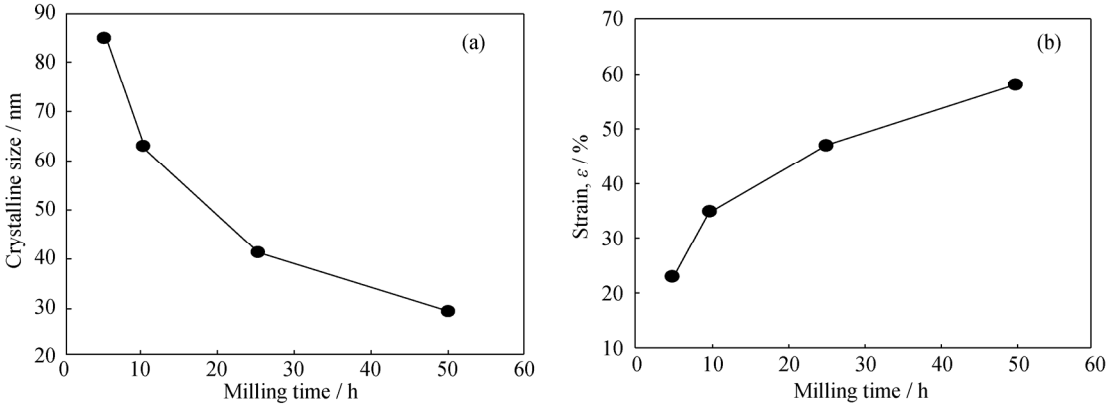

Fig. 3. Variation of (a) the crystalline size and (b) the lattice strain of the Cu matrix with milling duration.

An SEM image of the powder particles after mechanical alloying is shown in Fig. 4. After 50 h of mechanical alloying, the particle shape was irregular and the average particle size was approximately 50 μm. The variations in the morphology and size of powder particles are influenced by the diffusion of Cr, W, and Al_2O_3 particles into the Cu particles during the milling process. As evident in Fig. 4, few agglomerated particles were observed after ball milling. Achieving an equilibrium between cold welding and powder particles fracturing contributes to the prevention of agglomeration [22].

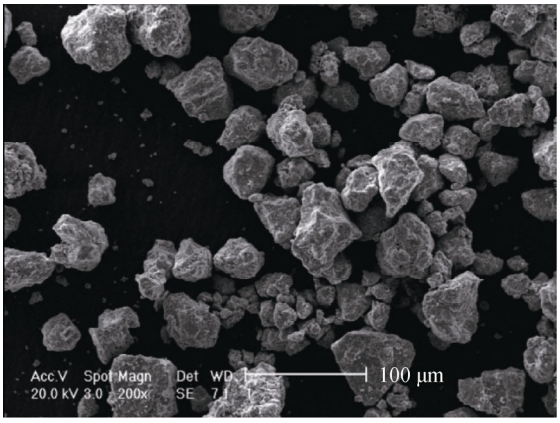

Fig. 4. Morphology of CuCrW(Al_2O_3) powder after 50 h of milling.

Fig. 5 presents the cross-sectional microstructure of the sintered samples. The microstructure of both samples indicates fine crack-free spherical pores in the grain boundaries, with no cracks observed. Similar results have been reported for specimens sintered using pulse electric current [23] and conventional sintering [24]. The grain boundaries' pores are more abundant in the CuCrW alloy microstructure. Al_2O_3 particles present in the metallic matrix may result in acceleration of the diffusion process and enhancement of the sintering conditions [25]. An explanation for this observation is that, in the process of metal–ceramic nanocomposite sintering, the size difference in components affects their diffusion coefficients and their sintering behaviors [26]. Components with finer sizes exhibit higher diffusion coefficients in nanocomposites and result in lower sintering temperatures [27]. Upon the addition of Al_2O_3 nanoparticles to the CuCrW alloy, the number of pores

located at the grain interfaces was reduced and the alloy's relative density increased. Similar results have been previously reported for sintered samples [28–30]. On the basis of the EDX analysis results shown in Fig. 6, the Al_2O_3, Cr, and W components were uniformly distributed in the Cu matrix. Therefore, the production of a CuCrW(Al_2O_3) nanocomposite is confirmed.

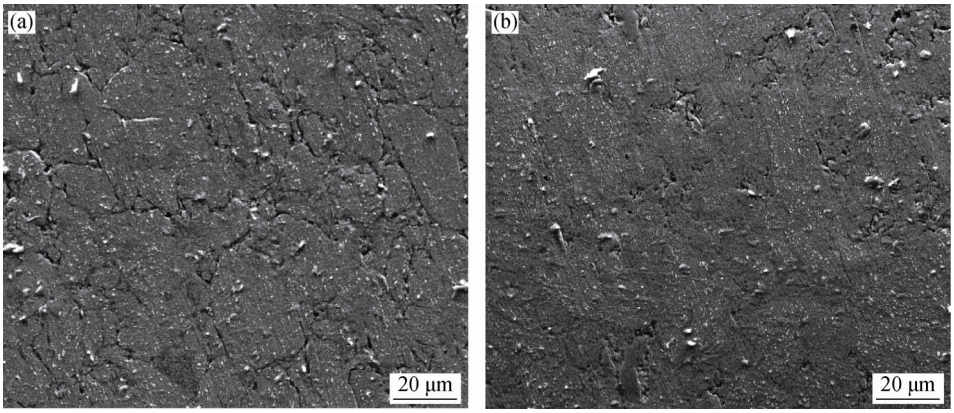

Fig. 5. SEM images of the cross-sectional microstructure of conventional sintered samples: (a) CuCrW; (b) CuCrW(Al_2O_3).

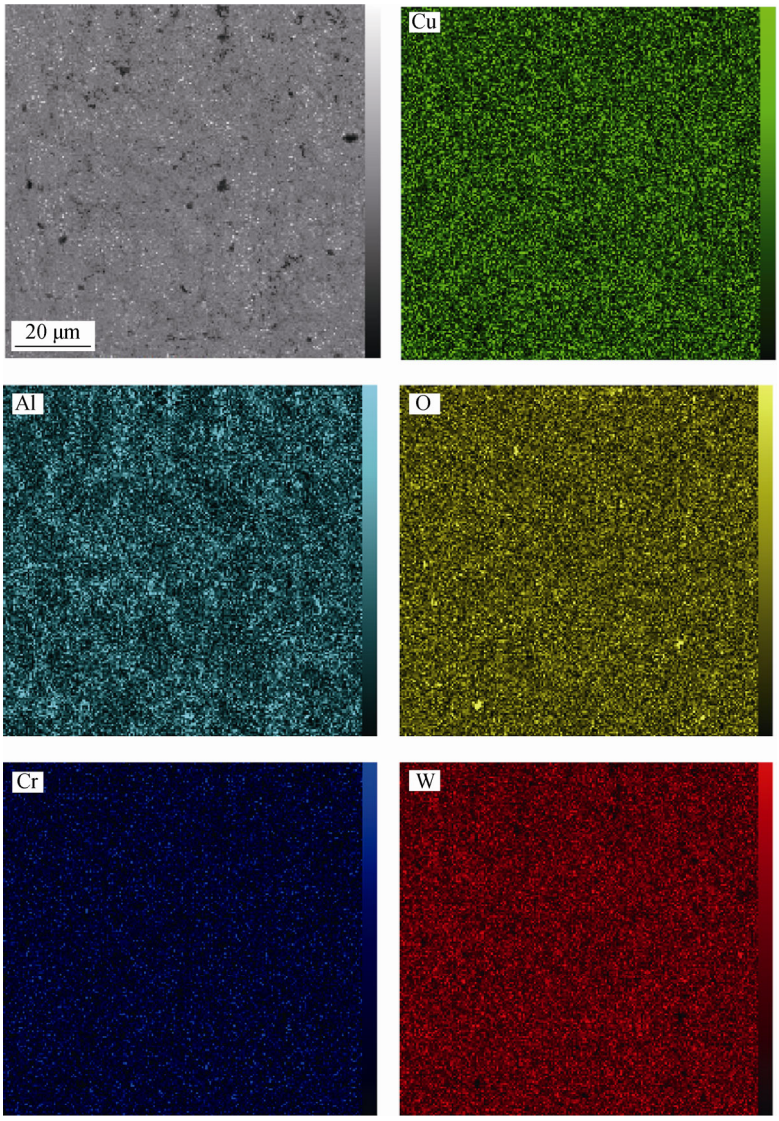

Fig. 6. SEM image and EDS distribution maps (Cu, Al, O, Cr, and W) for a conventionally sintered sample of the CuCrW(Al_2O_3) nanocomposite.

3.2. Relative density and hardness

Compared with theoretical density, the measured relative density before and after sintering of the CuCrW alloy and the CuCrW(Al_2O_3) nanocomposite were 91% and 95%, respectively (Table 3). Despite the presence of Al_2O_3 nanoparticles, the relative density of the alloy increased by 5%. Because of the prevalence of component-diffusion and particle-agglomeration processes, the sintered sample became denser [31]. The higher relative density of the CuCrW(Al_2O_3) nanocomposite might be attributable to the homogeneous distribution of Al_2O_3 nanoparticles and their position in the cavities located at the grain interfaces [29].

Table 3. Density of the CuCrW alloy and the CuCrW(Al_2O_3) nanocomposite prepared by conventional sintering

Sample	Relative density of green compact / %	Relative density of sintered sample / %
CuCrW	71	91
CuCrW(Al_2O_3)	69	95

The hardness of the sintered samples was measured (Table 4). These values are the mean of five hardness measurements. The hardnesses of the alloy and the nanocomposite were HV 335 and HV 368, respectively. As observed, the hardness of the alloys increased because of the presence of Al_2O_3 nanoparticles. This increase in hardness is attributable to dispersion hardening of the significantly hard Al_2O_3 nanoparticles in the CuCrW matrix [32]. The uniform distribution of hard Al_2O_3 nanoparticles, in contrast to the motion of dislocations, prevents plastic deformation of the CuCrW matrix under the applied load and increases the hardness [33–35]. Shehata *et al.* [36] studied the effect of adding Al_2O_3 nanoparticles to a Cu matrix. They observed that, upon the addition of 12.5wt% Al_2O_3 nanoparticles, the microhardness increased by 50% and reached HB 80.

Table 4. Microhardness of the CuCrW alloy and the CuCrW(Al_2O_3) nanocomposite prepared by conventional sintering

Sample	Hardness, HV
CuCrW	335 ± 7
CuCrW(Al_2O_3)	368 ± 4

3.3. Tribological behavior

3.3.1. Coefficient of friction properties

Figs. 7 and 8 show the curves of coefficient of friction (COF) for the CuCrW alloy and the CuCrW(Al_2O_3) nanocomposites, respectively, at sliding rates of 1 and 5 $m \cdot s^{-1}$. The mean values of two iterations were calculated at each step of the test procedure. The results show that the COF tends to increase with increasing sliding distance in most of the tests. İnitially, an oxide layer is present on the surface, which results in a lower COF at the beginning of the wear test. This oxide layer disappears during the wear test, which leads to an increase in either metal–metal contact or the adhesive wear. Furthermore, this phenomenon ultimately results in a higher COF [37]. In the meantime, as wear develops, a substantial amount of debris may enter the pin–disk contact zone. The presence of debris in this zone can lead to indirectly enhanced surface roughness as well as to an increase in the COF [38]. Fig. 7 shows that, in the wear tests on the alloy sample at both high and low sliding rates, the Al_2O_3 pin exhibited a higher COF. According to Table 1, the surface roughness of the Al_2O_3 pin is greater than those of steel and WC pins. Under such circumstances, asperity contact occurs between the pin and the disk, leading to the increased COF. The surface roughnesses of the steel and WC pins are relatively the same, but the WC pin is harder than the steel pin, which suggests that the WC pin should exhibit greater wear resistance [39]. Consequently, the steel pin is easily worn and may produce more wear debris particles. Therefore, the COF caused by steel-pin wear is greater than that of WC pins. Fig. 8 illustrates the results of wear tests on the nanocomposite, where the highest COF again corresponds to the Al_2O_3 pin and the lowest corresponds to the WC pin. As previously mentioned, the surface roughness of the Al_2O_3 pin is greater than those of the WC and steel pins. In this case, asperity contact occurs between the pin and the disk, increasing the COF. Despite the equal surface roughness of the steel and WC pins, the surface hardness of the steel pin is lower than that of the WC pin, which in turn results in less wear resistance [39]. Hence, more debris is produced by wearing through the steel pin, resulting in the increased COF. For both the alloy and the nanocomposite specimens, the COF also varies with the sliding rate. In this regard, with increasing sliding rate, the magnitude of the COF is mitigated. COF variation is likely due to changes in the wear mechanism [40]. At low sliding rates (Figs. 7(a) and 8(a)), the contact between the pin and disk becomes rougher and asperity contact occurs in the wear zone. With a decrease in sliding rate, the shear stress increases, which leads to an increase in COF [41]. On the contrary, at high sliding rates (Figs. 7(b) and 8(b)), this contact becomes smoother and the involvement between the pin and sample surface is diminished. The results show that the nanocomposite consistently exhibits a lower COF than the alloy sample. For example, a comparison of the average COFs for the

alloy at a sliding distance of 300 m reveals that the highest COF of 1.2, which was measured at a sliding rate of 1 m·s^{-1} using an Al_2O_3 pin, whereas the lowest COF was 0.79 and obtained with a WC pin at a sliding rate of 5 m·s^{-1}. For the nanocomposite, the highest and lowest COF were 1.15 and 0.61, which were achieved at sliding rates of 1 and 5 m·s^{-1} for steel and WC pins, respectively. Thus, the presence of Al_2O_3 nanoparticles in nanocomposite results in a decrease in COF.

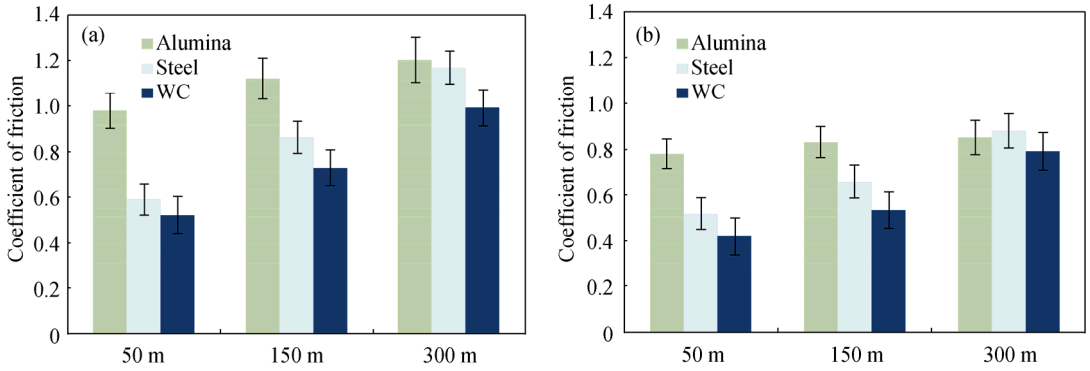

Fig. 7. Coefficient of friction for CuCrW alloy at three steps with different sliding rates using alumina, WC, and steel pins: (a) 1 m·s^{-1}; (b) 5 m·s^{-1}.

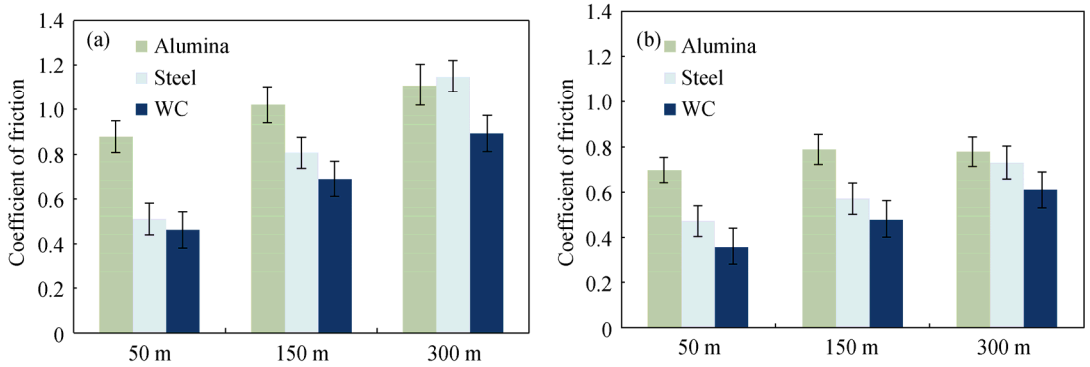

Fig. 8. Coefficient of friction for CuCrW(Al_2O_3) nanocomposite at three steps with different sliding rates using alumina, WC, and steel pins: (a) 1 m·s^{-1}; (b) 5 m·s^{-1}.

Similar results have been reported by Yasir *et al.* [42], Song *et al.* [43], and Hou and Chen [44]. These authors have stated that adding ceramic nanoparticles to a metal-based alloy caused a COF reduction in wear tests. The lower COF concerning the nanocomposite samples is attributable to a higher hardness than that exhibited by the alloy sample [45]. The reason for the increased hardness and reduced COF is the uniform distribution of Al_2O_3 nanoparticles in the alloy's matrix and the excellent bond between the matrix alloy and Al_2O_3 nanoparticles [46]. As vividly observed in Fig. 5, the microstructure of the nanocomposite sample is more uniform than that of the alloy sample. However, given the relative density results in Table 3, the microstructure uniformity and porosity reduction in the nanocomposite sample should lead to less debris triggered by wear and, thus, to a lower COF [47]. Because reinforcing ceramic particles act as a carrier, the severe contact area between the alloy surface and the abrasive pin reduces, which should lead to a decrease in COF values [48]. A lack of nanoparticles in the alloy surface also leads to a wider contact of the pin to the sample surface, the occurrence of a severe adhesive wear mechanism, and an increase in COF. Also, in the alloy sample, because of the lower hardness of the sample surface compared with that of the nanocomposite, debris caused by wear in the contact area of the pin and the sample is increased, leading to greater surface roughness in this area and, consequently, an increase in COF values.

3.3.2. Weight-loss rates

Fig. 9 demonstrates the weight-loss rates for the CuCrW alloy and the CuCrW(Al_2O_3) nanocomposite at sliding rates of 1 and 5 m·s^{-1}. The lowest weight loss rate for the alloy was 0.27 μg·N^{-1}·m^{-1} at a sliding rate of 5 m·s^{-1} and with a WC pin. By comparison, the greatest weight reduction amount was 0.59 μg·N^{-1}·m^{-1} at a sliding rate of 1 m·s^{-1} and with an Al_2O_3 pin. The lowest loss rate for the nanocomposite was 0.22 μg·N^{-1}·m^{-1} at a sliding rate of 5 m·s^{-1} and with

a WC pin, whereas the highest was 0.47 $\mu g \cdot N^{-1} \cdot m^{-1}$ at a sliding rate of 1 $m \cdot s^{-1}$ and with an Al_2O_3 pin. A comparison of the weight-loss rates in the alloy (Fig. 9(a)) and the nanocomposite (Fig. 9(b)) reveals that the presence of Al_2O_3 nanoparticles in the nanocomposite leads to a lower weight-loss rate. This increase in wear resistance of the nanocomposite with Al_2O_3 reinforcement nanoparticles is attributed to plastic deformation control [49].

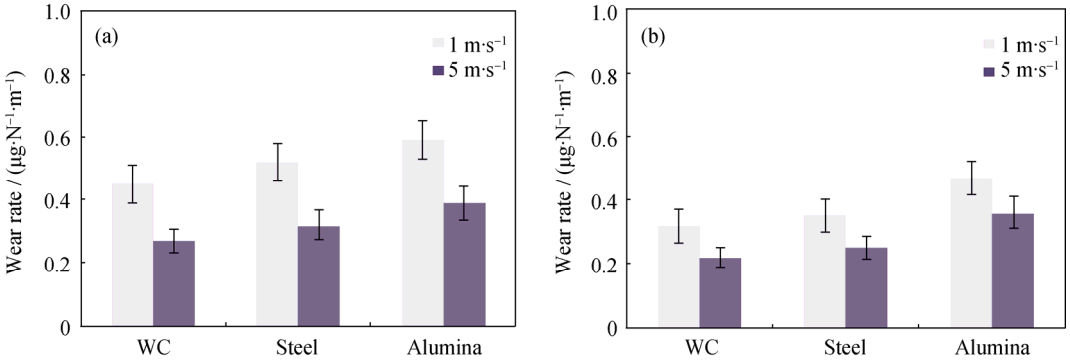

Fig. 9. Weight loss rates for (a) CuCrW alloy and (b) CuCrW(Al_2O_3) nanocomposite at three steps with the sliding rates of 1 and 5 $m \cdot s^{-1}$ using alumina, WC, and steel pins.

At a constant sliding rate, the weight-loss rate of the nanocomposite is lower than that of the alloy. Similar results have been reported in other studies [49–51]. According to the microstructure images in Fig. 5 and the relative density results, the microstructure of the nanocomposite was more uniform than that of the alloy and it exhibited a high relative density. That is, the nanocomposite structure was denser, and its surface was less porous. The microstructure uniformity and the porosity reduction in the case of the nanocomposite sample contribute to a smooth contact of the pin with the wear surface and, thus, to the generation of less wear debris [47]. The lower weight-loss rate of the nanocomposite may be related to its higher hardness, denser microstructure, and lower surface porosity compared with those of the alloy [45]. The uniform distribution of Al_2O_3 nanoparticles in the alloy matrix and an excellent bond between the matrix alloy and Al_2O_3 nanoparticles account for the hardness increase and weight-loss-rate decrease, respectively [46]. On the other side of the alloy sample, because of the lower hardness and greater porosity of the surface compared with the surface of the nanocomposite sample, the asperity contact of the pin is accompanied by a severe and harsh wear surface; consequently, the weight-loss rate increases. In the nanocomposite sample, with increasing sliding rate, the weight-loss rate increases. Because greater asperity contact occurs in the wear zone with increasing sliding rate, the shear stress increases, the bonds among particles are strengthened, the matrix of the alloy is fractured, and the reinforcement particles lose the capability to carry the load and separate from the surface. This phenomenon, in turn, leads to an increase in weight-loss rate [52].

A comparison of the results corresponding to the two investigated sliding rates reveals that the weight-loss rate resulting from Al_2O_3 pin wear is greater than the rates resulting from wear of the WC and steel pins. During the process of wear by the Al_2O_3 pin, because of the high surface roughness of this pin compared to those of the steel and WC pins (Table 1), contact occurs at the rougher wear zone; this contact leads to the further involvement between the pin and the wear surface and, accordingly, a higher weight-loss rate at both low and high sliding rates. The WC and steel pins exhibit lower surface roughness than the Al_2O_3 pin. That is, the WC and steel pins have smoother surfaces than the Al_2O_3 pin. These smoother surfaces should result in a lower weight-loss rate in wear tests using the WC and steel pins. However, in the case of the WC and steel pins, although pins with the same surface roughness should exhibit the same surface profile, the surface hardness of the WC pin is greater than that of the steel pin. This greater surface hardness of the WC pin compared with that of the steel pin could give rise to enhanced wear resistance. An explanation for this behavior is that less "pin deterioration debris generation" occurs on the wear surface and that the weight-loss rate during wear under the WC pin is lower than the weight-loss rates during wear under the steel and Al_2O_3 pins. Therefore, the WC pin provides better wear resistance.

For both samples, an alteration of the sliding rate resulted in changes in the weight-loss rate. With an increase in sliding rate in the pin-on-disk test, the rate of weight loss is reduced. As stated, at high sliding rates, the contact shear stress for the separation of material from the specimen surface is not adequate. However, at low sliding rates, rough

contact occurs in the wear zone, the shear stress is increased, and material is removed from the sample surface [41]. In addition, at high sliding rates, the friction process is elastic–plastic contact; thus, lowering the sliding rate and asperity contact results in increased plastic deformation [53]. Hence, reducing the sliding rate leads to detachment of the material from the sample surface and to an increase in weight-loss rate.

Figs. 10 and 11 illustrate the cross-sectional profiles of sliding distance for the CuCrW alloy and the CuCrW(Al_2O_3) nanocomposite at sliding rates of 1 and 5 $m \cdot s^{-1}$, respectively. The lowest depth of wear to the alloy was obtained at a sliding rate of 5 $m \cdot s^{-1}$ and with a WC pin. By contrast, the maximum depth of wear was obtained at a sliding rate of 1 $m \cdot s^{-1}$ and with an Al_2O_3 pin. In this regard, the lowest wear depth in the case of the nanocomposite was also achieved at a sliding rate of 5 $m \cdot s^{-1}$ and with a WC pin and the greatest wear depth also occurred at a sliding rate of 1 $m \cdot s^{-1}$ and with an Al_2O_3 pin. A comparison of the wear depth of the alloy sample (Fig. 10) with that of the nanocomposite sample (Fig. 11) reveals that the presence of Al_2O_3 nanoparticles in nanocomposites results in an increase in surface hardness and in plastic deformation control, leading to a mitigated abrasive pin diffusion in the specimen surface and decreased wear depth [49]. Moreover, the uniformity of the nanocomposite microstructure, together with its greater relative density compared with the alloyed sample, leads to smooth contact of the pin with the wear surface and, thus, reduced the depth of wear. Thus, the least wear depth developed in the nanocomposite samples can be attributed to higher hardness, a denser structure, and less porosity in the surface of the nanocomposite compared with that of the alloy [45]. For both samples at the same sliding rates, the depth caused by wear using an Al_2O_3 pin is always greater than those caused by the wear using WC and steel pins. The minimum wear depth is associated with wear by the WC pin. Again, for both samples, an increase in sliding rate resulted in diminished resultant wear depth. As previously mentioned, at a higher sliding rate, contact shear stress does not result in material separation from the surface. In comparison, at a lower sliding rate, asperity contact occurs at the wear zone, shear stress increases, and materials are separated from the sample surface [41].

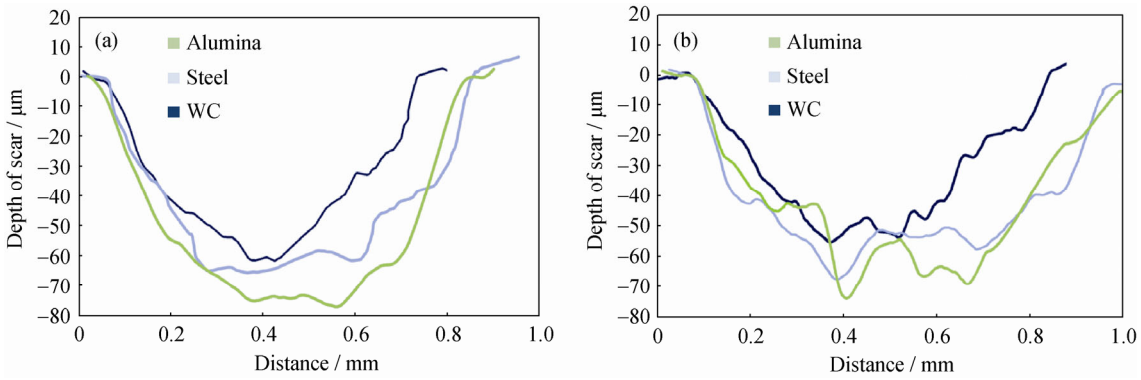

Fig. 10. Cross-sectional profiles of the sliding distance for CuCrW alloy after 300 m of sliding at different sliding rates using alumina, WC, and steel pins: (a) 1 $m \cdot s^{-1}$; (b) 5 $m \cdot s^{-1}$.

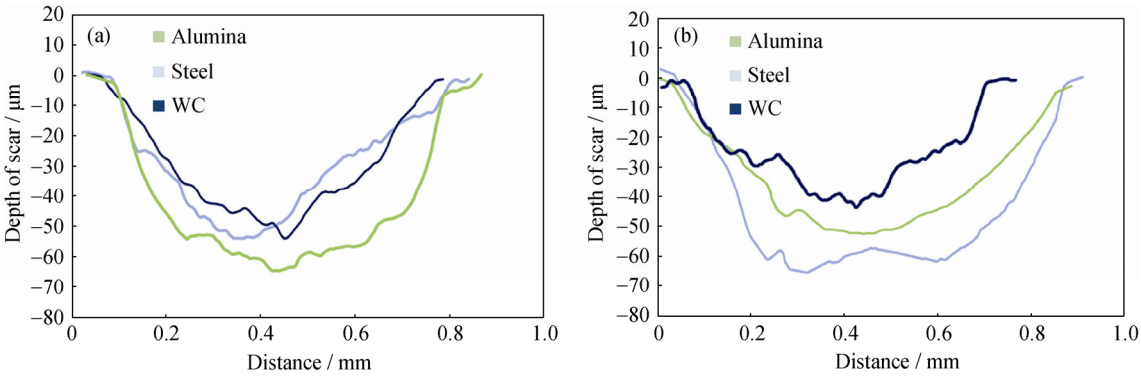

Fig. 11. Cross-sectional profiles of the sliding distance for CuCrW(Al_2O_3) nanocomposite after 300 m of sliding at different sliding rates using alumina, WC, and steel pins: (a) 1 $m \cdot s^{-1}$; (b) 5 $m \cdot s^{-1}$.

The surface profiles are consistent with the observed weight-loss rates. The wear process refers to the loss of material from the surface. Two important wear mechanisms explain the abrasive and adhesive types. Abrasive wear refers to surface damage caused by the placement of hard particles between the contact surfaces. These hard particles may originate from the contact parts or from the environment. The abrasive wear grade increases with increasing applied load and increasing the hardness of hard particles. Abrasive wear, which occurs as two involved surfaces slide against each other, generates localized connections, their failure, and eventually material detachment from the surface. The failure of connections at the interface or in a severe mode at the depth of the junction occurs constantly [54–55].

3.3.3. Evaluation of worn surfaces and wear mechanism

To investigate the mechanism of wear, we analyzed the SEM images of wear surfaces. Figs. 12 and 13 present the respective wear surfaces for the CuCrW(Al_2O_3) nanocomposite and the CuCrW alloy at different sliding rates. As shown in Fig. 12, in the wear surface of the nanocomposite sample at sliding rates of 1 and 5 m·s^{-1}, deep scratches and small cracks were observed, where the abrasive wear mechanism was detected. In Fig. 13, severe adhesion effects were observed in the alloy's wear surface. This phenomenon exhibits localized adhesion between the sample surface and the pin surface. A comparison of the wear-surface images reveals that, in the nanocomposite and the alloy samples, dominant mechanisms are abrasive and adhesive wear, respectively. Adhesive wear includes extensive surface damage and severe separation of materials from the surface. In the case of abrasive wear, separation of material from the surface occurs by a plowing process. This mechanism requires pin diffusion to the sample surface, which is controlled by the surface hardness [56]. Therefore, the weight-loss

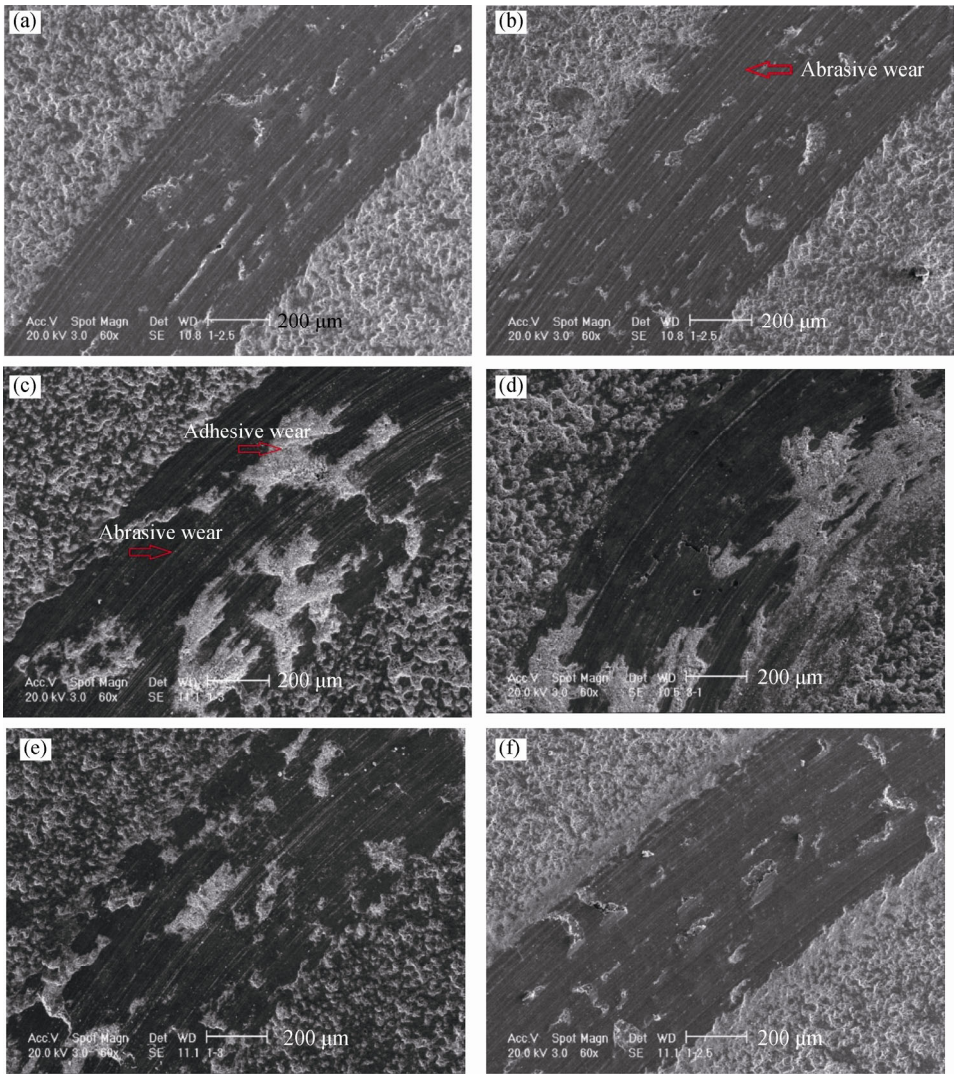

Fig. 12. SEM micrographs for the worn surface of the CuCrW(Al_2O_3) nanocomposite after 300 m of sliding: an Al_2O_3 pin with sliding rates of (a) 1 and (b) 5 m·s^{-1}; a steel pin with sliding rates of (c) 1 and (d) 5 m·s^{-1}; a WC pin with sliding rates of (e) 1 and (f) 5 m·s^{-1}.

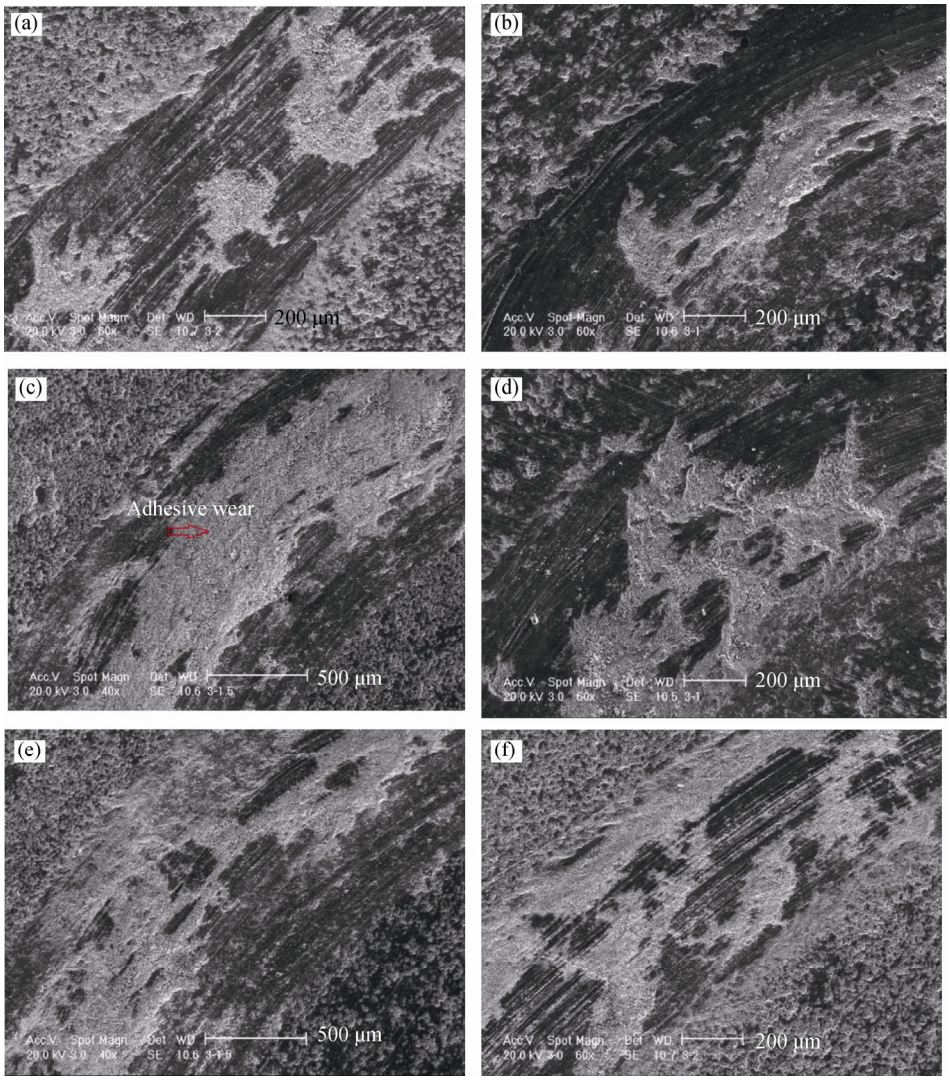

Fig. 13. SEM micrographs for the worn surface of the CuCrW alloy after 300 m of sliding: an alumina pin with sliding rates of (a) 1 and (b) 5 m·s^{-1}; a steel pin with sliding rates of (c) 1 and (d) 5 m·s^{-1}; a WC pin with sliding rates of (e) 1 and (f) 5 m·s^{-1}.

rate is inversely related to sample hardness, which in turn strongly affects the resistance to abrasive wear. As shown in Table 4, because of the Al_2O_3 nanoparticles, the nanocomposite exhibits higher hardness than the alloy. These results lead to the conclusion that the presence of Al_2O_3 nanoparticles in the alloy matrix leads to a change in the wear mechanism from abrasive to adhesive mode. Thus, the nanocomposite sample is expected to exhibit greater resistance to wear. This behavior is also consistent with the results of the weight-loss rate experiments and the cross-sectional SEM images. Similar results have been reported in other studies [57–59], where an inverse relationship was observed between hardness and the weight-loss rate in wear tests. Hence, the alloy sample exhibits greater porosity than the nanocomposite sample, leading to greater involvement between the wear pin and the disk surface wear and also greater detachment.

The authors of previous studies have reported that abrasive wear is the dominant wear mechanism in metal–matrix composites with a hard reinforcement material [60–61]. In this regard, Zhang *et al.* [62] stated that the severity of adhesive wear decreases with decreasing COF in a Cu–Ni alloy. Ding *et al.* [63] showed that the existence of Al_2O_3 reinforcement nanoparticles in a Cu-based alloy matrix leads to minor changes in the wear mechanism. For nanocomposites with 1wt% of Al_2O_3, the wear mechanism was adhesive, whereas abrasive wear was observed for the one containing greater than 2wt% of Al_2O_3. In Fig. 12, a mixture of adhesive and abrasive wear by steel and WC pins was observed on the wear surface of the nanocomposite sample (Fig. 12(c)). The creation of adhesive wear justifies the use of a metallic pin and metal-to-metal contact at the wear zone [63]. A comparison of the wear surfaces shown in Figs. 12(c) and 12(d)

reveals that the adhesive wear decreases with increasing sliding rate. An explanation for this observation is that, with an increase in sliding rate, the contact at the wear zone changes from rough to smooth and, subsequently, less connection and localized involvement between the pin and the disk surface occur. However, a comparison of Fig. 12(c) and Fig. 12(e) shows that a lower grade of abrasive wear occurs for the WC pin, likely because the higher hardness of the WC pin compared to that of the steel pin provides higher wear resistance. Fig. 13 shows that, in the case of wear of the alloy by steel and WC pins, severe abrasive wear occurred. Under these circumstances, the load was fully transferred to the disk by rough contact. Because of metal-to-metal contact and localized connection, greater adhesive wear occurs in wear tests with a metallic pin. In addition, by comparing wear images at low and high rates, the number of detachments indicating adhesive wear decreases during the wear carried out at a higher rate.

4. Conclusions

In this study, CuCrW SS was prepared after 50 h of mechanical alloying. Upon the addition of 5vol% Al_2O_3 nanoparticles to the CuCrW alloy, the hardness was increased by 10%. The tribological properties of the samples were evaluated using pin-on-disk wear tests. The comparison considered the damage mechanisms, wear, and friction between sintered samples and pins composed of different materials (Al_2O_3, WC, and steel 52100). The results indicate that WC pins exhibit a lower coefficient of friction than the Al_2O_3 and steel pins because of their high hardness and low surface roughness. A comparison of the weight-loss rates in the CuCrW alloy and the CuCrW(Al_2O_3) nanocomposite revealed that the existence of Al_2O_3 nanoparticles in the nanocomposite led to a lower weight-loss rate. In addition, a reduction in sliding rate led to the detachment of material from the sample surface and an increased weight-loss rate. With respect to the damage mechanism, the presence of Al_2O_3 nanoparticles in the alloy matrix led to a change in the wear mechanism from adhesive to abrasive wear.

References

[1] J.R. Davis, *Copper and Copper Alloys*, ASM International, Ohio, 2001, p. 246.

[2] E. Ma, Alloys created between immiscible elements, *Prog. Mater. Sci.*, 50(2005), No. 4, p. 413.

[3] C.Y. Zhang, Z.M. Yang, Y.P. Wang, B.J. Ding, and Y. Guo, Preparation of CuCr25 contact materials by vacuum induction melting, *J. Mater. Process. Technol.*, 178(2006), No. 1-3, p. 283.

[4] M. Bizjak, B. Karpe, G. Jakša, and J. Kovač, Surface precipitation of chromium in rapidly solidified Cu–Cr alloys, *Appl. Surf. Sci.*, 277(2013), p. 83.

[5] J. Gao, Y.P. Wang, Z.M. Zhou, and M. Kolbe, Phase separation in undercooled Cu–Cr melts, *Mater. Sci. Eng. A*, 449-451(2007), p. 654.

[6] Q. Zhao, Z.B. Shao, C.J. Liu, M.F. Jiang, X.T. Li, R. Zevenhoven, and H. Saxén, Preparation of Cu–Cr alloy powder by mechanical alloying, *J. Alloys Compd.*, 607(2014), p. 118.

[7] Q. Fang and Z.X. Kang, An investigation on morphology and structure of Cu–Cr alloy powders prepared by mechanical milling and alloying, *Powder Technol.*, 270(2015), p. 104.

[8] C. Aguilar, D. Guzmán, F. Castro, V. Martínez, F. de las Cuevas, S. Lascano, and T. Muthiah, Fabrication of nanocrystalline alloys Cu–Cr–Mo super satured solid solution by mechanical alloying, *Mater. Chem. Phys.*, 146(2014), No. 3, p. 493.

[9] S. Sheibani, S. Heshmati-Manesh, and A. Ataie, Influence of Al_2O_3 nanoparticles on solubility extension of Cr in Cu by mechanical alloying, *Acta Mater.*, 58(2010), No. 20, p. 6828.

[10] X.H. Yang, Z.K. Fan, S.H. Liang, and P. Xiao, Effects of TiC on microstructures and properties of CuW electrical contact materials, *Rare Met. Mater. Eng.*, 36(2007), No. 5, p. 817.

[11] X. Yang, Z. Fan, S. Liang, and P. Xiao, Effects of Y_2O_3 on properties of Cu–W electrical contact materials, *Chin. J. Mater. Res.*, 21(2007), No. 4, p. 414.

[12] P. Bacal, P. Indyka, Z. Stojek, and M. Donten, Unusual example of induced codeposition of tungsten. Galvanic formation of Cu–W alloy, *Electrochem. Commun.*, 54(2015), p. 28.

[13] T. Raghu, R. Sundaresan, P. Ramakrishnan, and T.R. Rama Mohan, Synthesis of nanocrystalline copper–tungsten alloys by mechanical alloying, *Mater. Sci. Eng. A*, 304-306(2001), p. 438.

[14] L. Xu, M. Yan, Y. Xia, J.H. Peng, W. Li, L.B. Zhang, C.H. Liu, G. Chen, and Y. Li, Influence of copper content on the property of Cu–W alloy prepared by microwave vacuum infiltration sintering, *J. Alloys Compd.*, 592(2014), p. 202.

[15] D.Y. Ying and D.L. Zhang, Processing of Cu–Al_2O_3 metal matrix nanocomposite materials by using high energy ball milling, *Mater. Sci. Eng. A*, 286(2000), No. 1, p. 152.

[16] L.S. Raju and A. Kumar, A novel approach for fabrication of Cu–Al_2O_3 surface composites by friction stir processing, *Procedia Mater. Sci.*, 5(2014), p. 434.

[17] W.M. Haynes, *CRC Handbook of Chemistry and Physics*, CRC Press, Florida, 2014, p. 251.

[18] B.D. Cullity, *Elements of X-ray Diffraction,* 2nd Ed., Adisson-Wesley Publishing, Boston, 1978, p. 368.

[19] H.P. Klung and L.E. Alexander, *X-ray Diffraction Procedures*, Willey, New York, 1962, p. 491.

[20] J. Eckert, J.C. Holzer, C.E. Krill, and W.L. Johnson, Reversible grain size changes in ball-milled nanocrystalline Fe–Cu alloys, *J. Mater. Res.*, 7(1992), No. 8, p. 1980.

[21] N.K. Mukhopadhyay, D. Mukherjee, S. Bera, I. Manna, and R. Manna, Synthesis and characterization of nano-structured

Cu–Zn γ-brass alloy, *Mater. Sci. Eng. A*, 485(2008), No. 1-2, p. 673.

[22] L. Lü and M.O. Lai, *Mechanical Alloying*, Springer Science & Business Media, Berlin, 2013, p. 346.

[23] R. Ritasalo, X.W. Liua, O. Söderberg, A. Keski-Honkola, V. Pitkänen, and S.P. Hannula, The microstructural effects on the mechanical and thermal properties of pulsed electric current sintered Cu–Al_2O_3 composites, *Procedia Eng.*, 10(2011), p. 124.

[24] D.G. Cho, S.K. Yang, J.C. Yun, H.S. Kim, J.S. Lee, and C.S. Lee, Effect of sintering profile on densification of nano-sized Ni/Al_2O_3 composite, *Composites Part B*, 45(2013), No. 1, p. 159.

[25] P.J.F. Harris, Growth and structure of supported metal catalyst particles, *Int. Mater. Rev.*, 40(1995), No. 3, p. 97.

[26] R.M. German, *Sintering Theory and Practice*, Wiley-VCH, New York, 1996, p. 568.

[27] R.M. German, *Powder Metallurgy and Particulate Materials Processing: the Processes, Materials, Products, Properties, and Applications*, Metal Powder Industries Federation, Princeton, 2005, p. 122.

[28] M. Korać, Ž. Kamberović, Z. Anđić, M. Filipović, and M. Tasić, Sintered materials based on copper and alumina powders synthesized by a novel method, *Sci. Sinter.*, 42(2010), No. 1, p. 81.

[29] S.H. Ryu, J.H. Park, C.S. Lee, J.C. Lee, S.H. Ahn, and S.T. Oh, Experimental measurement of coefficient of thermal expansion for graded layers in Ni–Al_2O_3 FGM joints for accurate residual stress analysis, *Mater. Trans.*, 50(2009), No. 6, p. 1553.

[30] Z. Hussain and H.K. Koay, Studies on alumina dispersion-strengthened copper composites through ball milling and mechanical alloying method, *J. Teknologi A*, 43(2005), p. 1.

[31] D.G. Kim, G.S. Kim, S.T. Oh, and Y.D. Kim, The initial stage of sintering for the W–Cu nanocomposite powder prepared from W–CuO mixture, *Mater. Lett.*, 58(2004), No. 5, p. 578.

[32] G. Di Girolamo, A. Brentari, C. Blasi, and E. Serra, Microstructure and mechanical properties of plasma sprayed alumina-based coatings, *Ceram. Int.*, 40(2014), No. 8, p. 12861.

[33] S. Alirezaei, S.M. Monirvaghefi, M. Salehi, and A. Saatchi, Effect of alumina content on surface morphology and hardness of Ni–P–Al_2O_3(α) electroless composite coatings, *Surf. Coat. Technol.*, 184(2004), No. 2-3, p. 170.

[34] Q.Y. Feng, T.J. Li, H.Y. Yue, K. Qi, F.D. Bai, and J.Z. Jin, Preparation and characterization of nickel nano-Al_2O_3 composite coatings by sediment co-deposition, *Appl. Surf. Sci.*, 254(2008), No. 8, p. 2262.

[35] H. Gül, F. Kiliç, S. Aslan, A. Alp, and H. Akbulut, Characteristics of electro-co-deposited Ni–Al_2O_3 nano-particle reinforced metal matrix composite (MMC) coatings, *Wear*, 267(2009), No. 5-8, p. 976.

[36] F. Shehata, M. Abdelhameed, A. Fathy, and M. Elmahdy, Preparation and characteristics of Cu–Al_2O_3 nanocomposite, *Open J. Met.*, 1(2011), No. 2, p. 25.

[37] G. Straffelini and A. Molinari, Effect of hardness on rolling–sliding damage mechanisms in PM alloys, *Powder Metall.*, 44(2001), No. 4, p. 153.

[38] H. Khorsand, S.M. Habibi, H. Yoozbashizadea, K. Janghorban, S.M.S. Reihani, H.R. Seraji, and M. Ashtari, The role of heat treatment on wear behavior of powder metallurgy low alloy steels, *Mater. Des.*, 23(2002), No. 7, p. 667.

[39] G. Straelini and A. Molinari, Dry sliding wear of ferrous PM materials, *Powder Metall.*, 44(2001), No. 3, p. 248.

[40] Z.F. Zhang, L.C. Zhang, and Y.W. Mai, Wear of ceramic particle-reinforced metal-matrix composites. Part II A model of adhesive wear, *J. Mater. Sci.*, 30(1995), No. 8, p. 1967.

[41] R. Ritasalo, M. Antonov, R. Veinthal, and S.P. Hannula, Comparison of the wear and frictional properties of Cu matrix composites prepared by pulsed electric current sintering, *Proc. Est. Acad. Sci.*, 63(2014), No. 1, p. 62.

[42] M. Yasir, C. Zhang, W. Wang, P. Xu, and L. Liu, Wear behaviors of Fe-based amorphous composite coatings reinforced by Al_2O_3 particles in air and in NaCl solution, *Mater. Des.*, 88(2015), p. 207.

[43] B. Song, S.J. Dong, H.L. Liao, and C. Coddet, Microstructure and wear resistance of FeAl/Al_2O_3 intermetallic composite coating prepared by atmospheric plasma spraying, *Surf. Coat. Technol.*, 268(2015), p. 24.

[44] K.H. Hou and Y.C. Chen, Preparation and wear resistance of pulse electrodeposited Ni–W/Al_2O_3 composite coatings, *Appl. Surf. Sci.*, 257(2011), No. 15, p. 6340.

[45] M.A. El-Hadek and S. Kaytbay, Al_2O_3 particle size effect on reinforced copper alloys: an experimental study, *Strain*, 45(2009), No. 6, p. 506.

[46] M. Knechtel, H. Prielipp, H. Müllejans, N. Claussen, and J. Rödel, Mechanical properties of Al/Al_2O_3 and Cu/Al_2O_3 composites with interpenetrating networks, *Scripta Metall. Mater.*, 31(1994), No. 8, p. 1085.

[47] A.A. Hamid, P.K. Ghosh, S.C. Jain, and S. Ray, The influence of porosity and particles content on dry sliding wear of cast *in situ* Al(Ti)–Al_2O_3(TiO_2) composite, *Wear*, 265(2008), No. 1-2, p. 14.

[48] S. Guicciardi, C. Melandri, F. Lucchini, and G. de Portu, On data dispersion in pin-on-disk wear tests, *Wear*, 252(2002), No. 11-12, p. 1001.

[49] A.G. Tang, M.L. Wang, W. Huang, and X.L. Wang, Composition design of Ni–nano-Al_2O_3–PTFE coatings and their tribological characteristics, *Surf. Coat. Technol.*, 282(2015), p. 121.

[50] N.K. Shrestha, K. Sakurada, M. Masuko, and T. Saji, Composite coatings of nickel and ceramic particles prepared in two steps, *Surf. Coat. Technol.*, 140(2001), No. 2, p. 175.

[51] M. Farvizi, T. Ebadzadeh, M.R. Vaezi, H.S. Kim, and A. Simchi, Effect of nano Al_2O_3 addition on mechanical properties and wear behavior of NiTi intermetallic, *Mater. Des.*, 51(2013), p. 375.

[52] K. Rajkumar and S. Aravindan, Tribological performance of microwave sintered copper–TiC–graphite hybrid composites, *Tribol. Int.*, 44(2011), No. 4, p. 347.

[53] S.Z. Wen and P. Huang, *Principles of Tribology*, John Wiley & Sons, New Jersey, 2002, p. 172.

[54] N. Govindarajan and R. Gnanamoorthy, Study of damage mechanisms and failure analysis of sintered and hardened steels under rolling–sliding contact conditions, *Mater. Sci. Eng. A*, 445-446(2007), p. 259.

[55] Y. Gao, J.C. Jie, P.C. Zhang, J. Zhang, T.M. Wang, and T.J. Li, Wear behavior of high strength and high conductivity Cu alloys under dry sliding, *Trans. Nonferrous Met. Soc. China*, 25(2015), No. 7, p. 2293.

[56] K. Kato, *Classification of Wear Mechanisms/Models*, John Wiley & Sons, New Jersey, 2005, p. 9.

[57] B. Yao, Z. Han, Y.S. Li, N.R. Tao, and K. Lu, Dry sliding tribological properties of nanostructured copper subjected to dynamic plastic deformation, *Wear*, 271(2011), No. 9-10, p. 1609.

[58] Z. Han, L. Lu, and K. Lu, Dry sliding tribological behavior of nanocrystalline and conventional polycrystalline copper, *Tribol. Lett.*, 21(2006), No. 1, p. 45.

[59] Y.S. Zhang, Z. Han, K. Wang, and K. Lu, Friction and wear behaviors of nanocrystalline surface layer of pure copper, *Wear*, 260(2006), No. 9-10, p. 942.

[60] I. Apachitei and J. Duszczyk, Autocatalytic nickel coatings on aluminium with improved abrasive wear resistance, *Surf. Coat. Technol.*, 132(2000), No. 1, p. 89.

[61] B. Bozzini, M. Boniardi, A. Fanigliulo, and F. Bogani, Tribological properties of electroless Ni–P/diamond composite films, *Mater. Res. Bull.*, 36(2001), No. 11, p. 1889.

[62] X.Y. Zhang, Y. Ma, N.M. Lin, X.B. Huang, R.Q. Hang, A.L. Fan, and B. Tang, Microstructure, antibacterial properties and wear resistance of plasma Cu–Ni surface modified titanium, *Surf. Coat. Technol.*, 232(2013), p. 515.

[63] G.H. Zhou, H.Y. Ding, Y. Zhang, D. Hui, and A.H. Lui, Fretting behavior of nano-Al_2O_3 reinforced coppermatrix composites prepared by coprecipitation, *Metalurgija*, 15(2009), No. 3, p. 169.